web of semantic

Journal of Interdisciplinary Science

Research Article Peer-review, Open Access

Optimization of Cabin Air Distribution in the Airbus A320 Using Computational Fluid Dynamics and Response Surface Methodology

Emmanuel Udama Odeh [1], Emenike Peculiar Akachukwu[2]

Abstract

Cabin air distribution in narrow-body aircraft must provide adequate mixing without producing excessive draught or leaving weakly ventilated pockets near seats and sidewalls. This study optimized the airflow response of an Airbus A320 economy-class cabin section using CFD coupled with Response Surface Methodology. A 24-run design varied inlet velocity (0.20-0.60 m/s), inlet temperature (20.0-25.0 °C), seat spacing (0.70-0.90 m) and mesh refinement (100,000-150,000 cells). The average cabin velocity ranged from 0.10 to 0.27 m/s, while maximum cabin temperature ranged from 22.7 to 28.0 °C. ANOVA showed that inlet velocity dominated the velocity response ($F = 5122.59$, $p < 0.0001$), with seat spacing also significant ($F = 21.52$, $p = 0.0035$). The fitted velocity model was highly consistent with the CFD results ($R^2 = 0.9991$; RMSE = 0.0019 m/s). Multi-response desirability predicted an operating point at 0.201 m/s inlet velocity, 20.595 °C inlet temperature, 0.709 m seat spacing and 150,000 cells, giving a predicted average velocity of 0.099 m/s and maximum temperature of 24.275 °C. Velocity contours showed where low-speed pockets tended to appear, but no cell-counted low-velocity area or volume fraction was computed. The predicted setting is therefore reported as a candidate for confirmatory CFD and detailed full-cabin evaluation, not as a final ECS operating prescription.

Keywords: Airbus A320; cabin airflow; computational fluid dynamics; response surface methodology; environmental control system; airflow optimization.

[1,2] *Department of Mechanical and Aerospace Engineering, University of Uyo, Uyo, Akwa Ibom State, Nigeria*

1. Introduction

Aircraft environmental control systems supply conditioned fresh and recirculated air within a compact and densely occupied cabin volume. The design task is not limited to meeting air-exchange and pressurization requirements; it also involves distributing momentum and heat in a way that avoids dead zones, local draught and temperature peaks [1,2].

Passenger response depends on local air temperature, air speed and turbulence rather than cabin-average values alone. Classical comfort theory gives a basis for interpreting local thermal sensation, but aircraft cabins remain difficult because seat rows, sidewalls and supply jets create strong spatial gradients over short distances [3,4].

Experimental airflow mapping remains important because it captures seat-row differences that may be missed by simplified models. However, repeated testing across many environmental-control-system settings is expensive. CFD offers a practical way to resolve velocity and temperature fields, provided that the numerical model, mesh and boundary conditions are stated clearly and interpreted within their limits [5-7].

Response Surface Methodology (RSM) is useful when a limited number of CFD simulations must be converted into a model that explains factor effects and interactions. Desirability optimization is also suitable when airflow and temperature objectives compete, because it allows the responses to be assessed together rather than by a single isolated variable [8,9].

Recent cabin studies show that local motion, inlet velocity and air-distribution strategy can substantially change contaminant pathways and occupant exposure. For that reason, CFD results are most useful when the flow physics, modelling assumptions and limits of interpretation are stated plainly [10-12].

The objective of this study is to optimize the average airflow response of an Airbus A320 economy-class cabin section while retaining thermal-performance control. The study combines CFD, RSM, ANOVA diagnostics and multi-response desirability to identify the flow variables that matter most before more expensive full-cabin simulations are attempted.

2. Materials and methods

2.1 Research process flowchart

The research process is summarized in Figure 1 and then described in the method subsections that follow. The work began with a defined airflow problem: the cabin section had to provide adequate bulk movement without implying that a single average velocity represents full airflow uniformity. The flowchart therefore separates the CFD solution from the response-evaluation stage, so that the velocity field is solved first and the average-velocity response is interpreted afterwards with its limitations stated clearly.

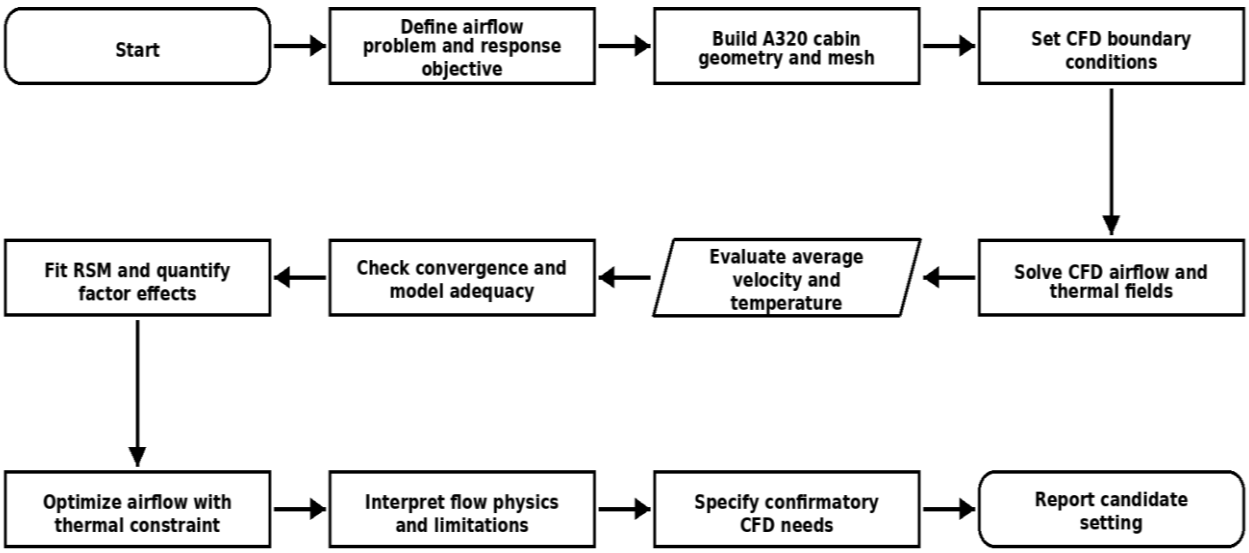

Figure 1. Standard research process flowchart for the airflow-focused CFD-RSM study.

After geometry construction and mesh generation, the CFD model was solved with the turbulence and energy models described below. The simulation outputs were screened for convergence and physical

consistency before response values were taken from the occupied-zone field. The RSM stage was then used to explain factor effects, test model adequacy and identify a predicted airflow setting that requires confirmatory CFD before practical use.

2.2 Cabin geometry, assumptions and boundary conditions

The computational domain represented a transverse Airbus A320 economy-class cabin section. The model retained the curved cabin envelope, seat-row blockage, main supply-air passages and outlet paths. Very small fixtures were not modelled because the objective was to compare parametric ECS responses rather than reproduce every cabin detail. This simplification keeps the simulation campaign repeatable while preserving the geometric features that most strongly affect flow acceleration, recirculation and thermal stratification.

The flow was treated as low-Mach-number cabin airflow. Air density was assumed constant except for buoyancy coupling in the thermal calculation. The cabin walls and seats were treated as stationary no-slip surfaces. The inlet boundary was prescribed by the design velocity and design temperature, while the outlet was treated as a pressure outlet. Seat spacing was varied as a cabin-layout parameter because seat rows alter the size of the local passages through which supplied air moves after entering the cabin section.

2.3 Mesh, solver settings and convergence control

Mesh refinement was included as a numerical-control factor and not as an ECS operating parameter. The mesh levels represented progressively refined tetrahedral discretizations from 100,000 to 150,000 cells. The mesh was assessed through quality indicators such as skewness and orthogonal quality, and the same response-evaluation procedure was used for all runs so that the parametric comparison remained consistent.

The simulations were performed with a pressure-based finite-volume formulation. The realizable k-epsilon turbulence model was used because it provides a stable and computationally efficient closure for repeated RANS simulations of indoor and cabin jets. The energy equation was activated to resolve the thermal field. Pressure-velocity coupling was handled iteratively, with second-order discretization used for the main transport equations where stable convergence was obtained. The residual targets were 10^-5 for continuity and momentum and 10^-6 for energy, together with monitored stabilization of average velocity and maximum temperature.

2.4 Governing equations and response surface formulation

The incompressible continuity equation, momentum equation, energy equation, second-order response surface and composite desirability function were expressed as follows:

$$\nabla \cdot u = 0 \quad (1)$$

$$\rho(u \cdot \nabla)u = -\nabla p + \mu\nabla^2 u + F \quad (2)$$

$$\rho Cp(u \cdot \nabla T) = k\nabla^2 T + Q \quad (3)$$

$$y = \beta 0 + \Sigma \beta i\, xi + \Sigma \beta ii\, xi\text{^}2 + \Sigma \beta ij\, xi\, xj + \varepsilon \quad (4)$$

$$D = (\Pi\, di\text{^}wi)\text{^}(1/\Sigma wi) \quad (5)$$

In the equations, u is the velocity vector, p is pressure, T is temperature, rho is air density, mu is dynamic viscosity, Cp is specific heat, k is thermal conductivity, Q is a volumetric heat source and F represents body-force effects. The RSM equation uses coded variables xi to allow direct comparison of factor effects, while the desirability function combines individual desirability values di using weights wi.

2.5 Experimental design, response evaluation and model adequacy checks

The response evaluation was performed after convergence by evaluating the volume-averaged air speed in the occupied cabin section and the maximum air temperature in the same domain. Average velocity

was used as a bulk airflow indicator, not as a complete airflow-uniformity index. Maximum temperature was used as a conservative thermal-performance response, not as a full PMV, PPD or draught-rate comfort index. Low-velocity regions were interpreted from velocity contours only; no area- or volume-integrated stagnant-zone fraction was calculated in this study.

Table 1. CFD-RSM design factors and investigated ranges.

Code	Factor	Range	Role in the analysis
A	Inlet velocity	0.20-0.60 m/s	Physical ECS supply-momentum factor
B	Inlet temperature	20.0-25.0 °C	Supply-air thermal factor
C	Seat spacing	0.70-0.90 m	Cabin-layout obstruction factor
D	Mesh refinement	100,000-150,000 cells	Numerical-control factor

The CFD design contained 24 runs. The fitted surfaces were assessed with ANOVA, coefficient estimates, residual diagnostics, R^2, RMSE and actual-predicted comparisons. The desirability optimum was treated as a model-predicted setting inside the investigated design space. Validation of that setting requires a separate CFD run carried out with the same geometry, boundary-condition definitions, turbulence model and mesh-quality checks.

For the airflow objective, average cabin velocity was selected as the primary response and maximum temperature was retained as a constraint response. This formulation prevents the optimization from favouring high supply momentum alone. The fitted model was interpreted together with the physical contour fields so that the outcome remained tied to cabin-flow behaviour rather than only to a statistical optimum.

The response evaluation procedure was deliberately kept separate from the flow solution step. After convergence, the velocity field was sampled within the occupied cabin section rather than at a single point. This avoided giving undue weight to local jet behaviour near the inlet and made the response more representative of the zone in which passengers experience the cabin microenvironment.

The average-velocity response was interpreted with caution. It describes the bulk movement of air through the modelled cabin section and not a full airflow-uniformity index. Low-velocity regions were therefore treated qualitatively from velocity contours. A quantified stagnant-zone assessment would require a fixed velocity threshold and a cell-counted area or volume fraction for both baseline and optimized cases.

Model adequacy was checked before optimization by examining ANOVA significance, residual error, R2, RMSE and actual-predicted agreement. The desirability step was then used only to identify a candidate airflow-control setting inside the investigated factor bounds. The final setting was not treated as a validated ECS design until confirmatory CFD at the predicted optimum is performed.

3. Results

3.1 CFD response range and airflow trend

Across the 24 simulations, the average cabin velocity varied from 0.10 to 0.27 m/s. The response increased mainly with inlet velocity, showing that supply momentum controlled the mean movement of air through the cabin section. Temperature and mesh refinement had comparatively small effects on the bulk velocity response, while seat spacing had a measurable secondary effect because it changed the local passage area around the seat row.

The trend in Figure 2 is an airflow-response trend rather than a comfort ranking. A higher average velocity can improve flushing in some regions, but it can also increase local draught if jets impinge directly on occupied zones. For this reason, the optimization did not simply maximize velocity; it selected a response that remained inside the modelled range while satisfying the thermal constraint.

Table 2. CFD-RSM design matrix and response outcomes.

Run	A: Inlet Velocity (m/s)	B: Inlet Temperature (°C)	C: Seat Spacing (m)	D: Mesh Refinement Level	Response 1: Average Cabin Velocity (m/s)	Response 2: Maximum Cabin Temperature (°C)
1	0.6	22.5	0.9	120,000	0.26	25.2
2	0.6	25	0.7	120,000	0.25	27.8
3	0.4	25	0.8	120,000	0.18	27.4
4	0.2	20	0.7	100,000	0.11	23.7
5	0.4	22.5	0.9	100,000	0.17	24.9
6	0.4	22.5	0.7	100,000	0.16	25.4
7	0.6	22.5	0.8	150,000	0.26	25.3
8	0.4	22.5	0.9	100,000	0.17	24.9
9	0.6	20	0.8	100,000	0.27	22.8
10	0.6	20	0.9	150,000	0.27	22.7
11	0.4	25	0.8	120,000	0.18	27.4
12	0.2	22.5	0.7	120,000	0.1	25.9
13	0.2	20	0.8	150,000	0.11	23.1
14	0.2	25	0.8	100,000	0.1	27.9
15	0.2	25	0.9	150,000	0.11	27.7
16	0.2	25	0.9	120,000	0.11	27.7
17	0.2	20	0.7	120,000	0.1	23.7
18	0.4	25	0.7	150,000	0.17	28
19	0.2	25	0.8	150,000	0.1	27.9
20	0.6	20	0.7	120,000	0.25	23.7
21	0.4	25	0.7	120,000	0.17	28
22	0.2	20	0.8	120,000	0.11	23.1
23	0.4	22.5	0.7	100,000	0.16	25.4
24	0.6	25	0.9	100,000	0.25	27.1

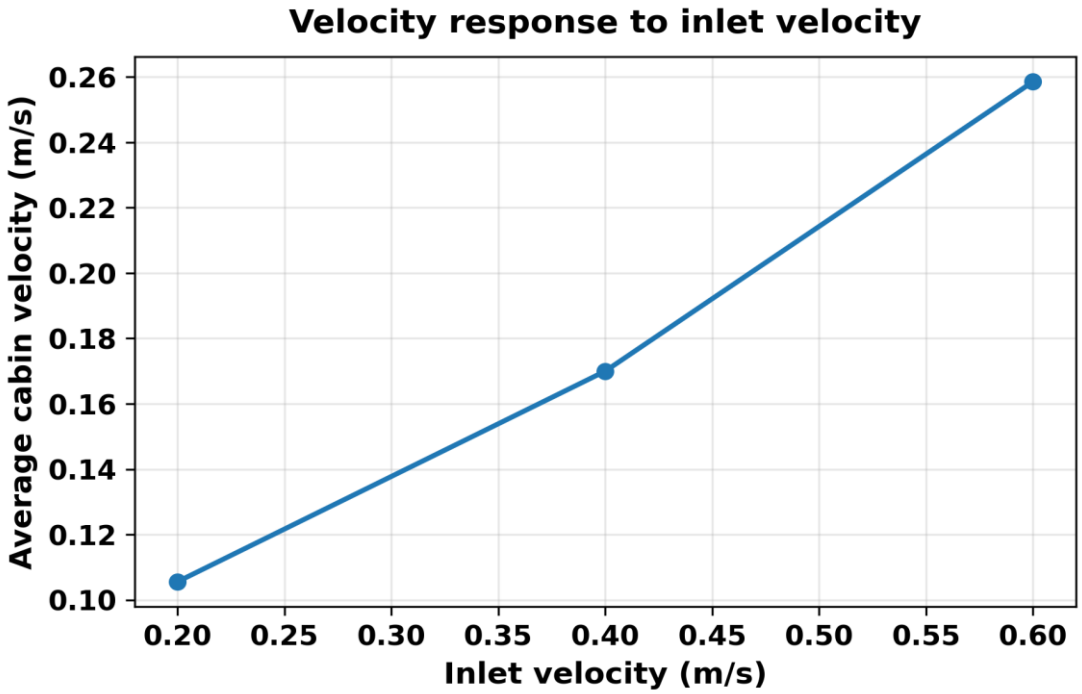

Figure 2. Mean average-cabin-velocity response at the investigated inlet-velocity levels.

3.2 Statistical influence of the design factors

The ANOVA result shows a clear hierarchy. Inlet velocity was the governing factor for average cabin velocity, while seat spacing produced a smaller but statistically significant contribution. Inlet temperature did not materially change the airflow response over the tested range. Mesh refinement had a limited effect on the fitted velocity response, suggesting that the simulated average velocity was not dominated by the numerical-resolution factor within the examined mesh range.

Table 3. ANOVA summary for the average cabin velocity response.

Source	Sum of Squares	Df	Mean Square	F-value	p-value	Unnamed: 6
Model	0.0932	17	0.0055	391.4	< 0.0001	significant
B-Inlet Temperature	1.00E-04	1	1.00E-04	4.76	0.0718	nan
C-Seat Spacing	3.00E-04	1	3.00E-04	21.52	0.0035	nan
D-Mesh Refinement Level	1.00E-04	2	0	2.28	0.1831	nan
AB	5.92E-07	1	5.92E-07	0.0422	0.8440	nan

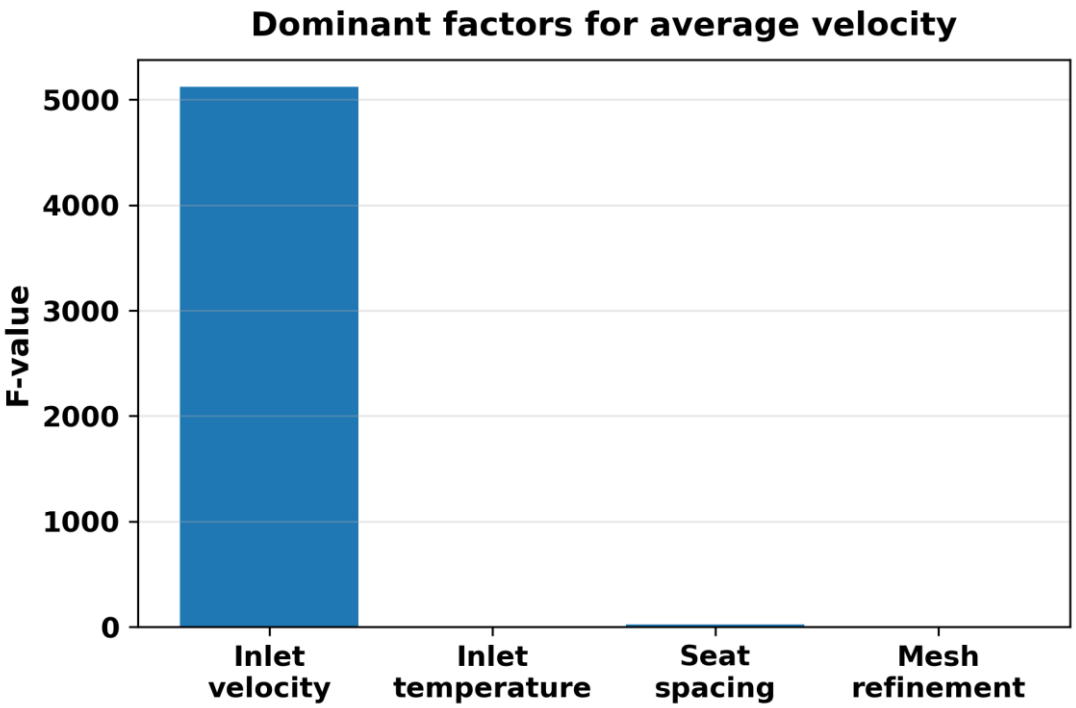

Figure 3. ANOVA F-values for the main factors affecting average cabin velocity.

3.3 Model diagnostics and desirability optimum

The diagnostic plot and tabulated residuals show that the fitted surface reproduced the available CFD points with low error. The high R^2 and small RMSE demonstrate interpolation quality within the tested design region, but they do not prove performance outside the design limits. The optimum was therefore treated as an RSM-predicted candidate and not as a replacement for a confirmatory CFD run.

Table 4. Representative actual-predicted diagnostics for average cabin velocity.

Run Order	Actual Value	Predicted Value	Residual	Leverage
1	0.26	0.2591	9.00E-04	0.94
2	0.25	0.2513	-0.0013	0.876
3	0.18	0.1794	6.00E-04	0.445
4	0.11	0.11	-0	0.941
5	0.17	0.1709	-9.00E-04	0.489
6	0.16	0.1609	-9.00E-04	0.489
7	0.26	0.2601	-1.00E-04	0.927
8	0.17	0.1709	-9.00E-04	0.489

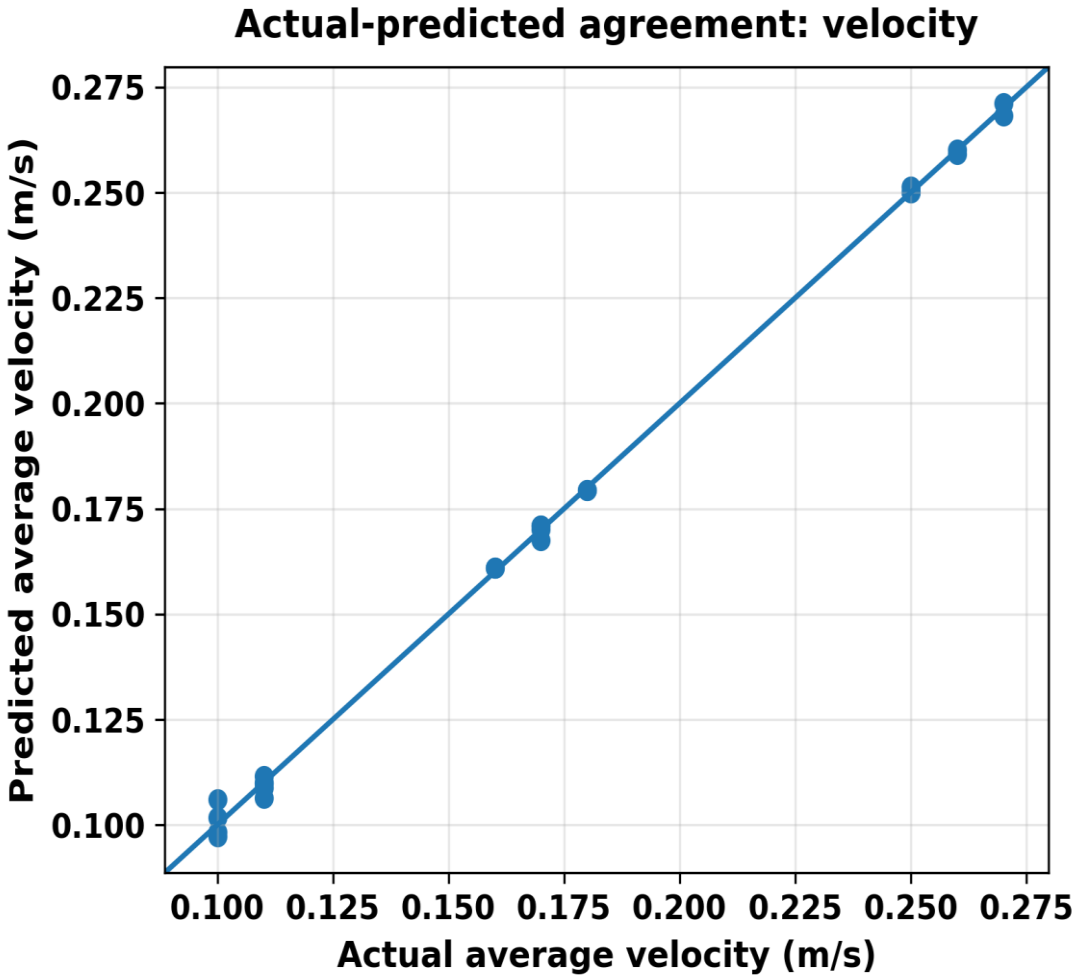

Figure 4. Actual-predicted agreement for the average cabin velocity response.

Table 5. Desirability-based optimum for airflow distribution with thermal-performance control.

Quantity	Value
Inlet velocity	0.201 m/s
Inlet temperature	20.595 °C
Seat spacing	0.709 m
Mesh refinement	150,000 cells
Predicted average cabin velocity	0.099 m/s
Predicted maximum cabin temperature	24.275 °C
Composite desirability	1.000

4. Discussion

The selected point lies close to the lower inlet-velocity bound because the objective emphasized airflow control without creating unnecessary thermal or draught risk. This is not a general argument for weak ventilation. Instead, it shows that, in this model, excessive supply momentum was not needed to achieve the target bulk velocity response when the thermal response was included in the desirability calculation.

The physical behaviour is consistent with flow through a blocked cabin section. The supply momentum moves air through narrow passages formed by the seat row and sidewall. When these passages are reduced, the local speed can rise in some channels while sheltered regions remain weakly ventilated. Seat spacing is therefore not merely a comfort-layout variable; it also alters the effective flow path seen by the ECS jets.

In practical cabin terms, the result means that a single cabin-average velocity value must be read together with the local flow paths. The inlet supplies the momentum, but the seat backs, cushion gaps and sidewall curvature decide where that momentum is spent. Some channels may carry most of the flow while adjacent sheltered pockets remain weakly flushed. For that reason, the optimization is best understood as a bulk airflow-control result, not as proof that every occupied-zone location receives the same air speed.

Low-velocity regions were assessed from the contour fields as an engineering observation. A limitation of the analysis is that no cell-integrated low-velocity area or volume fraction was computed. A quantitative confirmation would require a defined baseline case, a selected velocity threshold, and the same mesh and post-processing rule when comparing the baseline with the predicted optimum.

5. Conclusion

The CFD-RSM results show that average cabin velocity in the Airbus A320 cabin section is controlled mainly by inlet velocity, with seat spacing providing a meaningful secondary influence. The fitted model reproduced the 24 CFD runs with $R^2 = 0.9991$ and RMSE = 0.0019 m/s. The desirability analysis predicted an operating point of 0.201 m/s inlet velocity, 20.595 °C inlet temperature, 0.709 m seat spacing and 150,000 cells, with predicted responses of 0.099 m/s average velocity and 24.275 °C maximum temperature. The setting is best treated as a model-based candidate until an additional CFD run and a quantified low-velocity area or volume index confirm its performance.

References

1. Zhang, T., & Chen, Q. (2007). Novel air distribution systems for commercial aircraft cabins. Building and Environment, 42(4), 1675-1684. https://doi.org/10.1016/j.buildenv.2006.02.014
2. Liu, W., & Chen, Q. (2013). Current studies on air distributions in commercial airliner cabins. Theoretical and Applied Mechanics Letters, 3(6), 062001. https://doi.org/10.1063/2.1306201
3. Zhang, Z., Chen, X., Mazumdar, S., Zhang, T., & Chen, Q. (2009). Experimental and numerical investigation of airflow and contaminant transport in an airliner cabin mockup. Building and Environment, 44(1), 85-94. https://doi.org/10.1016/j.buildenv.2008.01.012
4. Mazumdar, S., & Chen, Q. (2009). A one-dimensional analytical model for airborne contaminant transport in airliner cabins. Indoor Air, 19(1), 3-13. https://doi.org/10.1111/j.1600-0668.2008.00553.x
5. Poussou, S. B., Mazumdar, S., Plesniak, M. W., Sojka, P. E., & Chen, Q. (2010). Flow and contaminant transport in an airliner cabin induced by a moving body: Model experiments and CFD predictions. Atmospheric Environment, 44(24), 2830-2839. https://doi.org/10.1016/j.atmosenv.2010.04.053
6. Liu, W., Wen, J., Lin, C. H., Liu, J., Long, Z., & Chen, Q. (2013). Evaluation of various categories of turbulence models for predicting air distribution in an airliner cabin. Building and Environment, 65, 118-131. https://doi.org/10.1016/j.buildenv.2013.03.018
7. Cao, X., Liu, J., Pei, J., Zhang, Y., Li, J., & Zhu, X. (2014). 2D-PIV measurement of aircraft cabin air

distribution with a high spatial resolution. Building and Environment, 82, 9-19. https://doi.org/10.1016/j.buildenv.2014.07.027

8. Dai, S., Sun, H., Liu, W., Guo, Y., Jiang, N., & Liu, J. (2015). Experimental study on characteristics of the jet flow from an aircraft gasper. Building and Environment, 93, 278-284. https://doi.org/10.1016/j.buildenv.2015.06.006
9. You, R., Chen, J., Shi, Z., Liu, W., Lin, C. H., Wei, D., & Chen, Q. (2016). Experimental and numerical study of airflow distribution in an aircraft cabin mock-up with a gasper on. Journal of Building Performance Simulation, 9(5), 555-566. https://doi.org/10.1080/19401493.2015.1126762
10. You, R., Chen, J., Lin, C. H., Wei, D., & Chen, Q. (2017). Investigating the impact of gaspers on cabin air quality in commercial airliners with a hybrid turbulence model. Building and Environment, 111, 110-122. https://doi.org/10.1016/j.buildenv.2016.10.018
11. You, R., Lin, C. H., Wei, D., & Chen, Q. (2019). Evaluating the commercial airliner cabin environment with different air distribution systems. Indoor Air, 29(5), 840-853. https://doi.org/10.1111/ina.12578
12. Wang, C., Liu, J., Li, J., Guo, Y., & Jiang, N. (2017). Turbulence characterization of instantaneous airflow in an aisle of an aircraft cabin mockup. Building and Environment, 116, 207-217. https://doi.org/10.1016/j.buildenv.2017.02.015
13. Zhang, Y., Liu, J., Pei, J., Li, J., & Wang, C. (2017). Performance evaluation of different air distribution systems in an aircraft cabin mockup. Aerospace Science and Technology, 70, 359-366. https://doi.org/10.1016/j.ast.2017.08.009
14. Li, J., Liu, J., Wang, C., Wesseling, M., & Muller, D. (2017). PIV experimental study of the large-scale dynamic airflow structures in an aircraft cabin: Swing and oscillation. Building and Environment, 125, 180-191. https://doi.org/10.1016/j.buildenv.2017.07.043
15. Li, J., Liu, J., Cao, X., & Jiang, N. (2016). Experimental study of transient air distribution of a jet collision region in an aircraft cabin mock-up. Energy and Buildings, 127, 786-793. https://doi.org/10.1016/j.enbuild.2016.06.039
16. Li, F., Liu, J., Ren, J., Cao, X., & Zhu, Y. (2016). Numerical investigation of airborne contaminant transport under different vortex structures in the aircraft cabin. International Journal of Heat and Mass Transfer, 96, 287-295. https://doi.org/10.1016/j.ijheatmasstransfer.2016.01.004
17. Maier, J., Marggraf-Micheel, C., Dehne, T., & Bosbach, J. (2017). Thermal comfort of different displacement ventilation systems in an aircraft passenger cabin. Building and Environment, 111, 256-264. https://doi.org/10.1016/j.buildenv.2016.11.017
18. Liu, M., Chang, D., Liu, J., Ji, S., Lin, C. H., Wei, D., Long, Z., Zhang, T., Shen, X., Cao, Q., & Chen, Q. (2021). Experimental investigation of air distribution in an airliner cabin mockup with displacement ventilation. Building and Environment, 191, 107577. https://doi.org/10.1016/j.buildenv.2020.107577
19. Liu, M., Liu, J., Cao, Q., Li, X., Liu, S., Ji, S., Lin, C. H., Wei, D., Shen, X., Long, Z., & Chen, Q. (2022). Evaluation of different air distribution systems in a commercial airliner cabin in terms of comfort and COVID-19 infection risk. Building and Environment, 208, 108590. https://doi.org/10.1016/j.buildenv.2021.108590
20. Yu, Z., Xiao, G., Zhang, C., Gui, Y., & Du, Y. (2022). Numerical study of air distribution and evolution characteristics in airliner cabin. Processes, 10(12), 2621. https://doi.org/10.3390/pr10122621
21. Shih, T. H., Liou, W. W., Shabbir, A., Yang, Z., & Zhu, J. (1995). A new k-epsilon eddy-viscosity model for high Reynolds number turbulent flows: Model development and validation. Computers &

Fluids, 24(3), 227-238. https://doi.org/10.1016/0045-7930(94)00032-T

22. Derringer, G., & Suich, R. (1980). Simultaneous optimization of several response variables. Journal of Quality Technology, 12(4), 214-219. https://doi.org/10.1080/00224065.1980.11980968